N, P Dual-Doped Carbons as Metal-Free Catalysts for Hydrogenation

Zhaoshuo Jiang,[∇] Yingchao Feng,[∇] Yu Gou, Ziyi Xia, Binwei Yuan, Syed Husnain Ali, Xuejiao Rong, Anni Guo, Ligong Chen, and Bowei Wang*

Cite This: *ACS Omega* 2024, 9, 40424−40432

Read Online

ACCESS | Metrics & More | Article Recommendations | Supporting Information

ABSTRACT: The activation of molecule hydrogen (H_2) by metal-free catalysts is always a challenge in the field of catalysis. Herein, a series of N, P dual-doped carbon catalysts were constructed by the pyrolysis of chitosan and phytic acid and utilized as metal-free catalysts for the hydrogenation of nitrobenzene. The characterization indicated that the doping of phosphorus atoms not only formed the species with catalytic activity for hydrogenation reaction but also promoted the doping of N. The experimental results indicated that their catalytic performance could be improved by the regulation of pyrolysis temperature and heating rate. CP-900−1 (pyrolysis at 900 °C with a heating rate of 1 °C/min) exhibited a promising catalytic activity with >99% nitrobenzene conversion. N, P codoping was the key factor to its catalytic performance. All results indicated that the excellent catalytic activity of CP-900−1 was attributed to the synergistic interaction among pyridinic N, P−C species, and graphitic N. This work provides an effective route for the rational design and construction of highly efficient metal-free catalysts for hydrogenation.
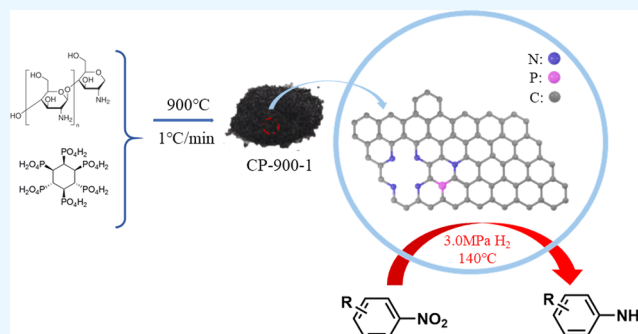
1. INTRODUCTION

Hydrogenation, as a crucial organic reaction, plays an irreplaceable role in many fields such as the synthesis of fine chemicals.[1−3] It uses cheap and easily available hydrogen gas as a reducing agent with excellent atomic economy, and it is regarded as the cleanest reduction method.[4] However, since hydrogen molecules are difficult to activate and normally cannot directly participate in the reaction, catalysts that can effectively activate hydrogen molecules are the key to this green process.[5] Designing and preparing catalysts with high activity and selectivity have always been significant challenges in the field of catalytic hydrogenation.

At present, many catalysts are employed in hydrogenation reactions. Although homogeneous catalysts can come into full contact with the reactant, they are problematic to separate from the reaction system.[6−8] Heterogeneous catalysts offer an ideal solution and can be reused multiple times, making them highly favored in industrial production.[9,10] Among them, metal-based catalysts exhibit outstanding catalytic activity for hydrogenation,[11−13] but they also have some inherent drawbacks including limited reserves and expensive prices of precious metals, as well as inevitable leaching and agglomeration of metal components, leading to catalyst activity reduction and product contamination.[14,15] For high-end fine chemicals like drugs and electronic chemicals, trace metal impurities can cause severe harm to products' quality. Therefore, developing efficient and stable metal-free catalysts can fundamentally solve the above shortcomings and has significant application value.

Metal-free catalysts are considered as potential alternatives to traditional metal catalysts because they do not undergo metal leaching due to the absence of metal active components.[16−18] Carbon materials are commonly used as good carrier materials for metal-based catalysts due to their wide range of sources and stable properties.[19,20] However, carbon materials are always catalytically inert for H_2 activation due to the regular structure and uniform surface charge distribution.[21] Doping heteroatoms (B, N, P, S) in carbon matrix is a convenient and effective modification strategy.[22,23] The doping of heteroatoms can induce electron transfer between heteroatoms and carbon atoms, as well as alter the charge distribution around carbon atoms and heteroatoms.[24,25] In addition, due to differences in atomic size, defects can be introduced into carbon materials during the doping process.[26] All of the above changes can endow the carbon material with catalytic activity for hydrogenation. At present, the research on carbon-based, metal-free catalysts is still in its infancy, mainly focusing on the construction of catalysts and the exploration of active sites. In spite of some progress that has been made, there remains no unified conclusion regarding the active site or a clear understanding of the specific H_2 activation mecha-
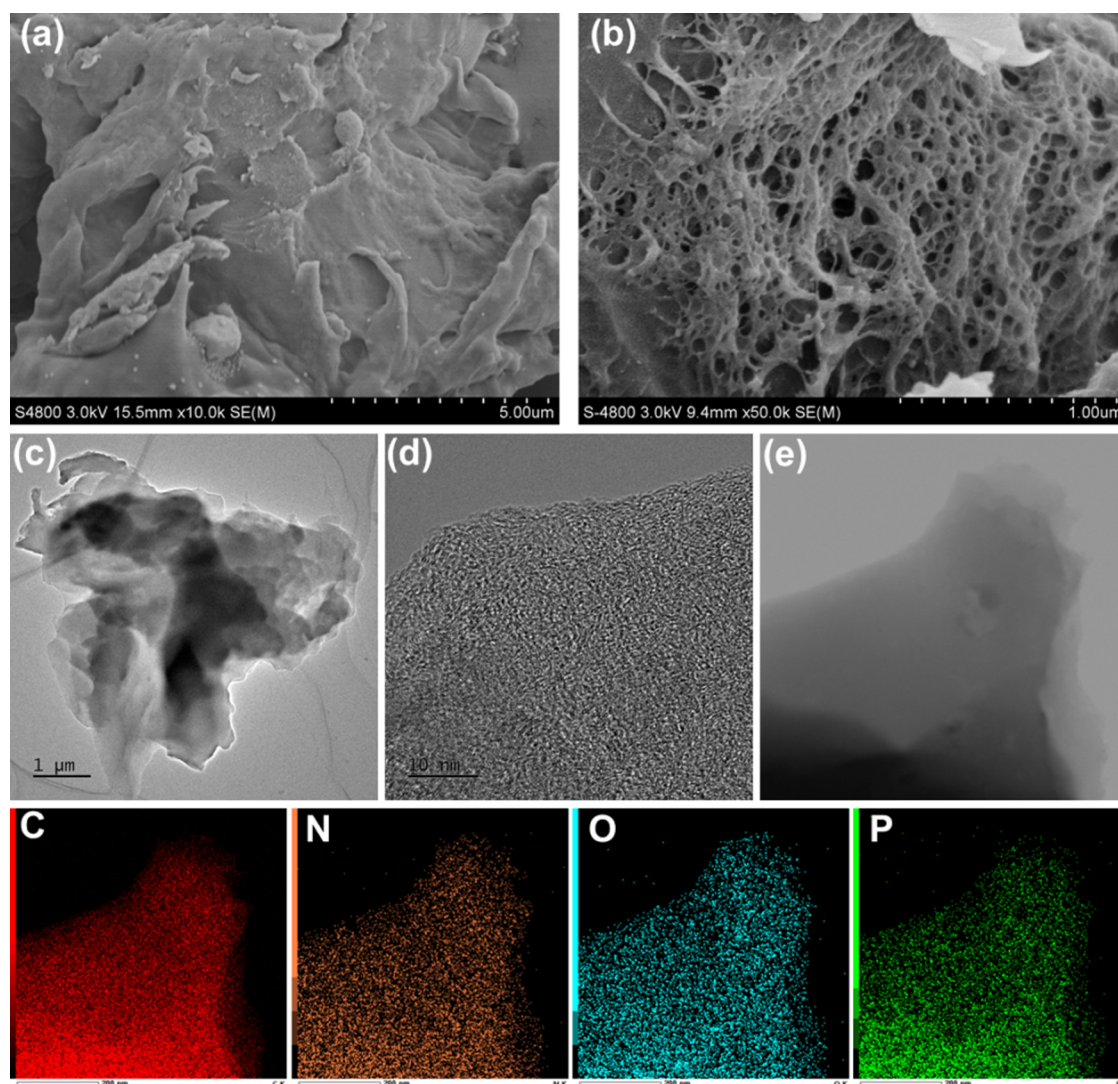
Figure 1. SEM images (a, b), TEM images (c, d), and EDX elemental maps (e) of CP-900−1 catalyst.

nism.[27−29] Although carbon materials doped with a single heteroatom of B, N, P, and S have been proven as promising catalysts for some hydrogenation reactions, their performance remains unsatisfactory, and harsh reaction conditions are necessary. For instance, Han et al.[30] prepared oxygen-induced zigzag graphene (OZG) via thermal treatment of rGO, which possessed high-performance activity with 99.7% nitrobenzene conversion. However, this conversion of nitrobenzene could only be achieved under the harsh conditions of 4 MPa H_2 and 170 °C. Codoping of multiple heteroatoms may be an effective approach to enhance the catalytic activity of carbon-based catalysts for hydrogenation due to the synergistic effect arising from the electronic interactions between different dopants.[31−34] Specifically, it is crucial to determine how different dopants simultaneously affect the activity of carbon materials as hydrogenation catalysts.

Herein, we have developed a series of biomass-derived N, P dual-doped carbon-based catalysts (CP-T-X, where T refers to the pyrolysis temperature and X refers to the heating rate) using chitosan as both the carbon and nitrogen source and phytic acid as the phosphorus source. The catalytic performance was evaluated by the hydrogenation of nitrobenzene to aniline. The content and doping forms of nitrogen and

phosphorus in the catalyst could be adjusted by changing the temperature and heating rate during pyrolysis. The relationship between the structure and activity of the catalyst was discussed according to the characterization and experimental results. Among all catalysts, CP-900−1 exhibited excellent catalytic activity for nitrobenzene hydrogenation, which should be attributed to its suitable content and doping form of nitrogen and phosphorus. What's more, doped P played a key role in N doping: doped P was beneficial for increasing the content of N doping, regulating the N configuration, and increasing the proportion of pyridinic N. It provides guidance for the rational design of metal-free catalysts.

2. EXPERIMENTAL SECTION

2.1. Materials. Chitosan and phytic acid were purchased from Shanghai Macklin Biochemical Technology Co., Ltd. Cellulose was obtained from Sinopharm Chemical Reagent Co., Ltd. Nitrobenzene was purchased from Rionlon Bohua (Tianjin) Pharmaceutical & Chemical Co., Ltd. Organic solvents were sourced from Tianjin Jiangtian Chemical Technology Co., Ltd. All reagents were used without further purification.
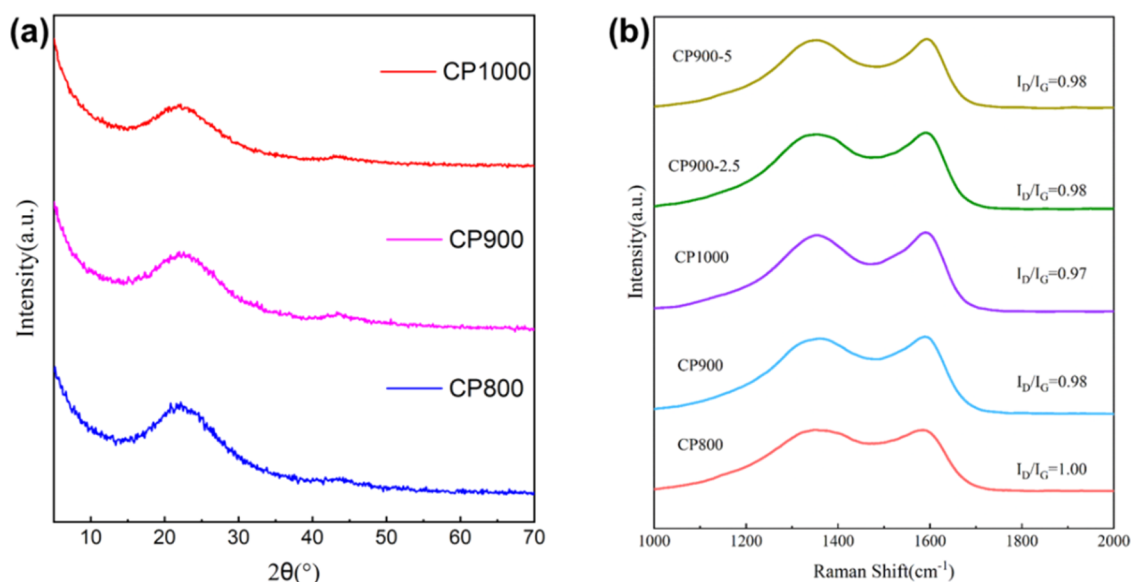
Figure 2. (a) XRD patterns and (b) Raman spectra of the prepared catalysts.

2.2. Catalyst Preparation. Initially, chitosan (2.5 g) and phytic acid (1.0 g) were added to ethanol aqueous solution (60 mL, 5:1, V/V) and stirred for 4 h. Subsequently, the solvent was gradually removed by rotary evaporator and dried in a vacuum oven at 60 °C for 6 h. The resulting solid was then pulverized into powder, followed by pyrolysis under Ar atmosphere at the designated temperature for 2 h with a specific heating rate to yield N, P dual-doped carbon catalysts denoted as CP-T-X (T represented the pyrolysis temperature, T = 800, 900, 950, 1000 °C. X denoted the heating rate, X = 1, 2.5, 5 °C min^{-1}). A similar procedure was employed to prepare single-doped carbon catalysts. P-900−1 was prepared with cellulose instead of chitosan, and N-900−1 was obtained from pure chitosan. In addition, C-900−1 without any heteroatom doping was prepared from pure cellulose. The preparation details of all catalysts are summarized in Table S1.

2.3. Evaluation of Catalysts. The hydrogenation of nitrobenzene to aniline was used as a probe reaction to evaluate the catalytic performance of the prepared materials. Typically, 0.25 mmol of nitrobenzene, 3 mL of solvent, and 30 mg of catalyst were added to a stainless-steel autoclave with a poly(tetrafluoroethylene) lining. The autoclave was purged 3 times with 1 MPa nitrogen and then 10 times with 1 MPa hydrogen to remove air from it. The reactor was then filled with hydrogen to 3 MPa and maintained at 200 °C for 3 h with magnetic stirring. After the reaction, the reaction mixture was cooled naturally to room temperature and analyzed by gas chromatography.

2.4. Characterization. The morphology and structure of the samples were observed by transmission electron microscopy (TEM, JEM-F200 from JEOL) and scanning electron microscopy (SEM, Regulus 8100 from HITACHI). Powder X-ray diffraction (XRD) patterns were recorded on a Smartlab (Rigaku, Japan) in the 2θ range of 5−80° (5°/min) with a Cu Kα source. Raman spectra were obtained on a Thermo FischerDXR spectrometer with an excitation wavelength of 532 nm. X-ray photoelectron spectroscopy (XPS) measurements were conducted on a Thermo ESCALAB 250Xi instrument to examine the elemental composition and forms. Elemental analysis (EA) was performed by using an Elementar

Unicube. Inductively coupled plasma optical emission spectra (ICP-OES) were collected by a Thermo Fisher iCAP PRO.

3. RESULTS AND DISCUSSION

3.1. Catalyst Characterization. The microstructure of the prepared samples was characterized by SEM and TEM. As shown in Figure S1 (a,b), the raw material chitosan exhibited a smooth, wavy structure, and no pore structure was observed under high magnification. After pyrolysis, N-900−1 displayed a slightly wrinkled surface with no obvious pore structure (Figure S1c,d). In sharp contrast, the samples pyrolyzed with phytic acid showed a curled and wrinkled structure. Figure S1(e,f) showed the SEM images of CP-800−1, from which it could be seen that there were a few fold structures on the surface of the sample, and some sparse pore structures could be observed after magnification. The surface of CP-900−1 (Figure 1a) exhibited dense and curled wrinkles, and a porous network structure could be observed. This phenomenon may be attributed to the decomposition of phosphoric acid groups on phytic acid, thereby facilitating the formation of a well-defined pore structure. Such porous structure was closely related to the high activity of the catalyst, which could expose more active sites and facilitate the mass transfer and substrate adsorption of the reaction.[32] The SEM image of CP-1000−1 is shown in Figure S1(i). Compared with CP-900−1, the wrinkles on its surface were reduced, and the overall surface became smoother. Moreover, no dense network structure was observed, which may be due to the collapse of the pore structure caused by excessive temperature. In addition, the samples were characterized by TEM. As shown in Figures 1c and S2, the samples prepared at different pyrolysis temperatures showed similar stacked lamellar structures in the TEM characterization. The amorphous carbon structure in the catalyst was confirmed by the presence of disordered curved stripes (Figure 1d). Moreover, energy-dispersive system (EDS) elemental images showed that the four elements of C, N, O, and P were evenly distributed on CP-900−1, confirming the successful doping of N and P (Figure 1e).

The XRD patterns were applied to analyze the crystal structures of the catalysts (Figure 2a). All catalysts exhibited
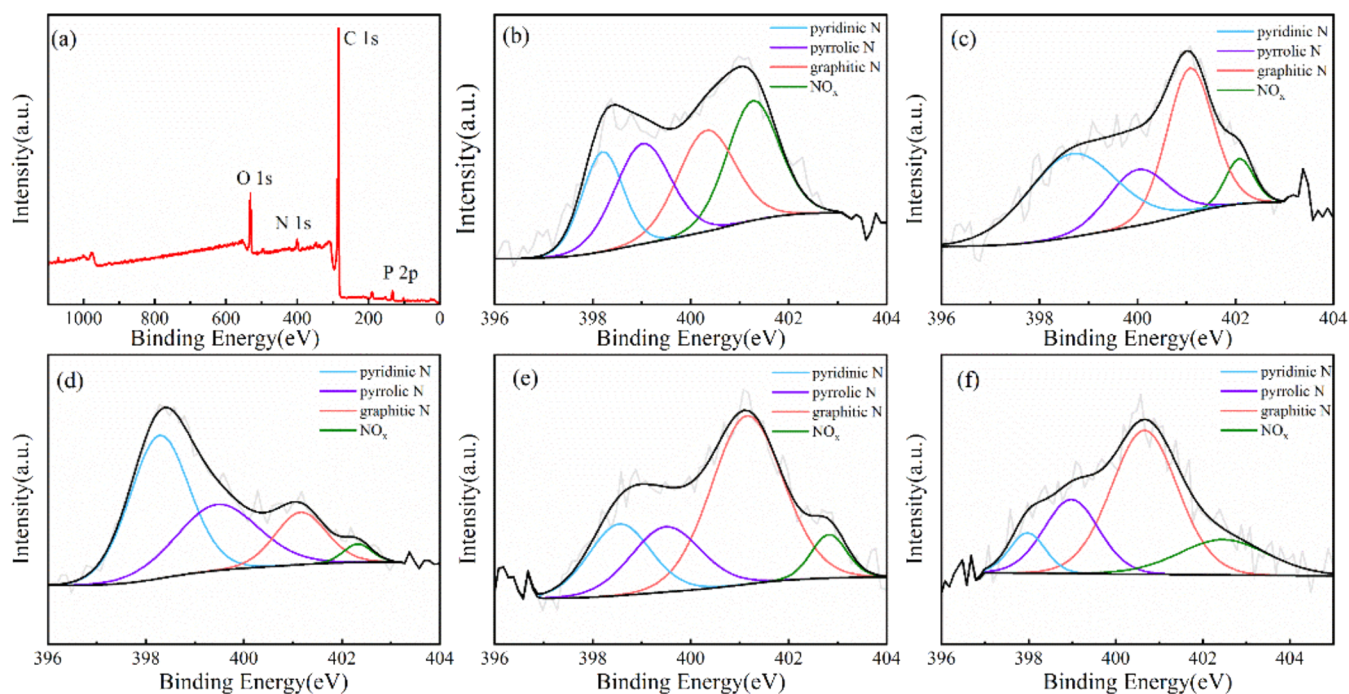
Figure 3. (a) XPS spectra of the CP-900−1 catalyst and XPS high-resolution N 1s of (b) CP-800−1, (c) CP-900−1, (d) CP-1000−1, (e) CP-900−2.5, and (f) CP-900−5.
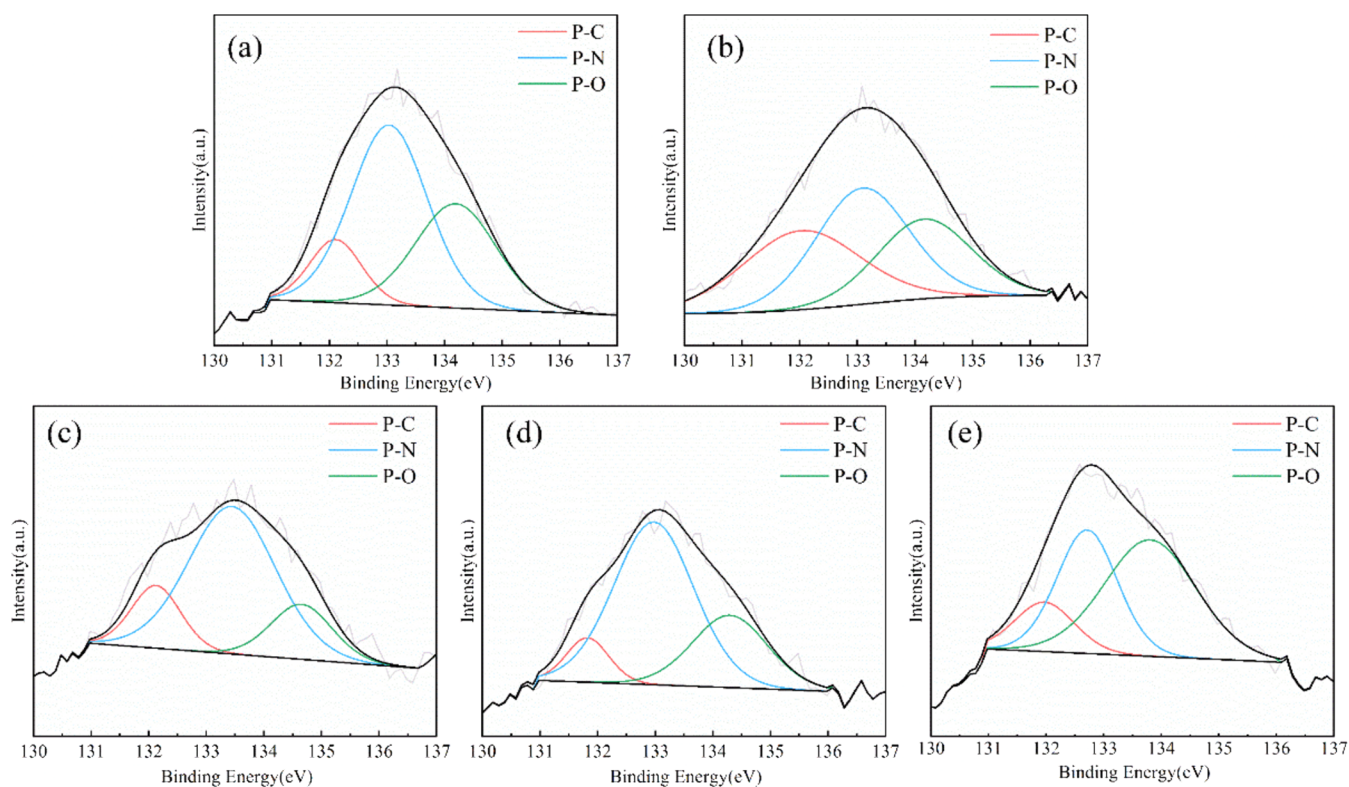
Figure 4. XPS high-resolution P 2p of (a) CP-800−1, (b) CP-900−1, (c) CP-1000−1, (d) CP-900−2.5, and (e) CP-900−5.

two broad peaks at approximately 23 and 43°, corresponding to (002) and (100) planes of graphite, respectively.[22] The presence of low-intensity broad peaks indicated the amorphous structure and partial graphitization of the catalysts, which was consistent with the TEM results. In addition, Raman spectra were employed to analyze the content of structural defects in the catalysts. Two peaks were observed at 1350 and 1580 cm^{-1}

in Figure 2b, corresponding to the characteristic D and G bands, respectively. The D band signifies sample disorderliness, while the G band characterizes the graphitization degree. Hence, the intensity ratio of I_D/I_G is commonly used to characterize the content of defects in carbon materials. A higher value of I_D/I_G indicates a higher defect content.[35] The I_D/I_G values remained unchanged at 0.98 as the heating rate

Table 1. Composition of Nitrogen and Phosphorus Species in Catalysts

catalyst	the relative content of nitrogen species (%)				the relative content of phosphorus species (%)		
	pyridinic N	pyrrolic N	graphitic N	NO$_x$	P—C	P—N	P—O
CP-800−1	18.80	25.81	26.70	28.69	12.89	53.99	33.11
CP-900-1	39.47	17.92	35.80	6.80	33.58	39.29	27.13
CP-950-1	37.55	29.57	27.12	5.76	19.36	58.03	22.61
CP-1000−1	49.66	31.60	15.68	3.06	15.97	66.61	17.42
CP-900−2.5	19.61	20.07	53.44	6.89	9.29	63.93	26.78
CP-900−5	7.88	22.32	52.52	17.28	13.92	35.39	50.69
N-900−1	26.46	11.73	61.80				
P-900−1					66.20		33.80

increased from 1 to 5 °C/min, indicating that the heating rate had no significant effect on the defect content in the catalyst. As the pyrolysis temperature increased from 800 to 1000 °C, the I_D/I_G value decreased from 1.00 to 0.97, suggesting a slight reduction in defect content.

The elemental composition and chemical status of the catalyst were investigated by X-ray photoelectron spectroscopy (XPS). As shown in Figure 3a, the catalyst contained C, N, O, and P, confirming the successful doping of N and P into the carbon matrix, which were also observed in energy-dispersive X-ray (EDX) results (Figure 1e). Numerous studies have demonstrated that the doping form of heteroatoms has a significant impact on the catalytic activity of catalysts.[15,28] To further elucidate the specific forms of nitrogen and phosphorus species, high-resolution N 1s and P 2p spectra were collected (Figures 3, 4, and S3). All of the samples contained four distinct nitrogen species: pyridinic N (398 eV), pyrrolic N (399 eV), graphitic N (400.5 eV), and nitrogen oxide (402 eV).[36,37] Previous studies have indicated that pyridinic N is beneficial to the dissociation of H$_2$ and serves as a potential activation site of H$_2$.[38,39] As the pyrolysis temperature increased, the proportion of nitrogen oxide in CP-*T*-*X* decreased, while the proportion of pyridinic N increased (Table 1). Meanwhile, as the heating rate increased, the content of nitrogen oxide increased, and the content of pyridinic N decreased. Under identical preparation conditions (pyrolysis temperature, 900 °C; heating rate, 1 °C/min), the proportions of different nitrogen species were significantly different between N-900−1 and CP-900−1. The proportion of pyridinic N was 26.46%, and the proportion of graphitic N was 61.80% in N-900−1. After doping phosphorus atoms in the nitrogen-doped carbon matrix, the pyridinic N of CP-900−1 increased to 39.47%, exhibiting the highest pyridinic N content among all catalysts, and the graphitic N proportion decreased to 35.80%. This indicated that the doped phosphorus atoms changed the doping mode of nitrogen atoms and significantly increased the content of pyridinic N.

The P 2p spectra of CP-*T*-*X* were fitted to three different peaks, including P—C (132.1 eV), P—N (133.2 eV), and P—O (134.1 eV) (Figure 4 and Table 1). As the pyrolysis temperature increased, the content of P—O decreased. Higher temperatures were conducive to the binding of P to carbon or nitrogen, thereby reducing the content of P—O. When the heating rate reached 5 °C/min, phosphorus mainly combined with oxygen, and the content of P—O in the catalysts increased significantly. Therefore, the excessive heating rate was not conducive to the doping of P into the carbon matrix. Among all of the CP-*T*-*X* materials, CP-900−1 displayed the highest content of P—C.

The elemental contents of the prepared catalysts are summarized in Table 2. With the increase of the pyrolysis

Table 2. Element Content of Catalysts

catalyst	C	H	O	N	P
CP-800−1	64.545	1.6035	21.7505	5.58	6.521
CP-900−1	68.305	1.679	23.276	3.085	3.655
CP-1000−1	72.415	1.6755	21.9545	1.915	2.040
CP-900−2.5	66.03	1.946	26.329	3.025	2.670
CP-900−5	64.17	2.2405	28.0805	2.72	2.789

temperature, the contents of nitrogen and phosphorus in the catalysts gradually decreased. This phenomenon was attributed to the fact that heteroatoms were more likely to overflow from the catalyst at a high temperature. At the pyrolysis temperature of 900 °C, the increased heating rate led to a significant decrease in phosphorus content within the catalyst. This phenomenon may be attributed to the relatively large atomic radius of P, which hinders its incorporation into the carbon matrix and requires a lower heating rate for sufficient doping content. In addition, as the heating rate increased, the nitrogen content gradually decreased, indicating that a lower heating rate was also conducive to nitrogen doping. Therefore, the appropriate heating rate and pyrolysis temperature were critical for sufficient nitrogen and phosphorus doping in the catalyst. When the pyrolysis was conducted at 900 °C with a heating rate of 1 °C/min, the nitrogen content of N-900−1 was 2.61%, while that of CP-900−1 increased to 3.09%. Without altering the initial nitrogen concentration in the precursor material, the nitrogen content of CP-900−1 significantly increased compared to that of N-900−1, suggesting that doped P could promote N doping and significantly increase the content of N.

The N$_2$ adsorption and desorption tests were employed to explore the specific surface area and porous structure of the catalysts, and the results are collected as shown in Table 3 and Figure S4. As shown in Figure S4a, all N$_2$ adsorption−desorption isotherms exhibited an unclosed characteristic. This phenomenon may be attributed to the unique pore structure of
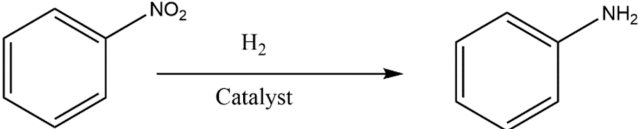
Table 3. Specific Surface Area and Pore Structure of Catalysts

catalyst	S_{BET} (m^2/g)	V_{total} (cm^3/g)	$D_{average}$ (nm)
N-900−1	284.58	0.23	12.38
CP-800−1	370.72	0.25	14.20
CP-900−1	540.98	0.42	15.63
CP-950−1	496.20	0.36	12.62
CP-1000−1	467.72	0.28	12.58

the carbon material, which hinders the desorption of the gas after adsorption, thus leading to the incomplete closure of the N_2 adsorption−desorption curves.[40] The pore size distribution curves showed that carbon materials have abundant micro- and mesoporous structures (Figure S4b). The specific surface area of N-900−1 was only 284.58 m^2/g, and that of CP-900−1 increased to 540.98 m^2/g. This may be attributed to the decomposition of phosphoric acid groups of phytic acid during the pyrolysis process, which could promote the formation of a rich pore structure (Table 3). When the pyrolysis temperature exceeded 900 °C, the specific surface area of the prepared samples showed a decreasing trend, which could be attributed to the collapse of the pore structure due to the excessively high temperature. The large specific surface area facilitated the generation and dispersion of active sites and contributed to the reaction's mass transfer.[32] Therefore, we hypothesize that the CP-900−1 catalyst may exhibit excellent catalytic activity.

3.2. Catalytic Hydrogenation of Nitrobenzene. The catalytic performance of the prepared catalysts was evaluated by employing the hydrogenation of nitrobenzene to aniline as the model reaction and H_2 as the hydrogen source (Table 4).

Table 4. Catalytic Performance of Catalysts[a]

entry	catalyst	conversion (%)
1		<1
2	C-900−1	<1
3	N-900−1	13.55
4	P-900−1	7.64
5	CP-700−1	1.78
6	CP-800−1	40.66
7	CP-900−1	>99
8	CP-950−1	41.77
9	CP-1000−1	6.30
10	CP-900−2.5	21.16
11	CP-900−5	1.43

[a]Conditions: 30 mg catalyst, 0.25 mmol nitrobenzene, 2.5 mL of mixed solvent (V_{EtOH}/V_{H_2O} = 3:2), 3 MPa H_2, 140 °C, 3 h.

It was evident that the conversion rate of the reaction was poor without a catalyst (entry 1). When C-900−1 was used as a catalyst (entry 2), nitrobenzene exhibited almost no reactivity, indicating that carbon materials without heteroatom doping were catalytically inert. By employing single nitrogen-doped N-900−1 and single phosphorus-doped P-900−1 as catalysts, the conversion of nitrobenzene was increased to 7.64 and 13.55%, respectively, indicating that both nitrogen and phosphorus doping could enhance the catalytic activity of carbon materials (entry 3, entry 4). However, this improvement remained relatively limited. CP-900−1 not only introduced phosphorus atoms into the carbon matrix but also significantly increased the total N content and pyridinic N content compared to N-900−1, resulting in a significant increase in the conversion rate of nitrobenzene, which could reach over 99% within 3 h (entry 7). This result confirmed the crucial promoting effect of doped P on N doping, which was beneficial for the formation of catalytic active species and thus enhanced the catalytic activity of the catalyst. As the pyrolysis temperature increased from
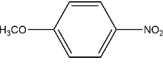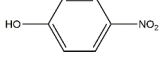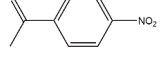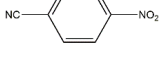
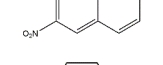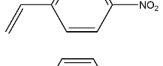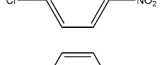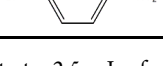700 to 1000 °C, the activity of CP-*T*-X catalysts initially exhibited an upward trend followed by a subsequent decline. The catalyst pyrolyzed at 900 °C exhibited the best catalytic performance, achieving nearly complete conversion of nitrobenzene. CP-700−1 catalyst displayed low activity, and the reaction was difficult to proceed over it (entry 5). This was because the lower pyrolysis temperature made it difficult for heteroatoms to be doped into the carbon lattice. However, as the pyrolysis temperature increased to 1000 °C, heteroatoms were more likely to overflow from the carbon lattice, resulting in a decrease in doping content and subsequent reduction in catalytic activity. Furthermore, the influence of heating rate was also investigated (entries 7, 10, 11). With the increase of heating rate, the content of heteroatoms in the catalyst decreased, leading to a reduction in its catalytic activity. Based on the aforementioned analysis, the dual-doping of N and P in the carbon matrix could significantly enhance the catalytic activity for hydrogenation. Moreover, both the doping amount and form of heteroatoms exhibited substantial impacts on catalyst performance. The presence of pyridinic N can alter the electronic structure of carbon materials, which is beneficial for the dissociation of hydrogen molecules.[38,41] In fact, the CP-900−1 catalyst with the highest pyridinic N content exhibited optimal catalytic performance, suggesting that pyridinic N may serve as the active site for activating H_2. Moreover, graphitic N could facilitate nitrobenzene adsorption by lowering the adsorption energy.[42] In addition, phosphorus atoms possess a relatively large atomic radius along with strong electron-donating ability.[26] After being doped into the carbon matrix, they could form a metal-like electronic structure, which was conducive to the activation of H_2 molecules. Through the analysis of the relationship between the different doping forms of phosphorus in Figure 4 and the conversion rate of nitrobenzene in Table 2, it could be concluded that CP-900−1 with the highest content of P−C exhibited the highest catalytic activity.

We further explored the effect of solvents on the hydrogenation reaction of nitrobenzene (Table S2). In an anhydrous reaction system, the reduction of nitrobenzene required more stringent reaction conditions for it to occur, resulting in a low conversion rate (entries 7−11). However, a higher conversion of nitrobenzene was achieved when water was used as the solvent (entry 6). Moreover, nitrobenzene was almost completely converted in the mixed solvent consisting of ethanol and water (entry 1), in which water molecules promoted H_2 dissociation by lowering its activation energy through the "H-shuttle" mechanism.[43] Meanwhile, the hydrogen bonds formed between the nitro group and water could effectively activate the N−O bond, further promoting the hydrogenation reaction.[43] Using water as the solvent led to a lower conversion of nitrobenzene compared to the water−ethanol mixed solvent. This could be attributed to the poor solubility of nitrobenzene in water, which affected the mass transfer process of the reaction, resulting in a lower conversion rate.

Hydrogenation of functional nitrobenzene derivatives to corresponding amino compounds is of great significance in the synthesis of fine chemicals.[44] Therefore, the catalytic hydrogenation of diverse substituted nitroarenes was examined with CP-900−1 (Table 5). Most of the nitroarenes bearing with different substituent groups exhibited favorable conversion. For alkyl-substituted nitrobenzenes, prolonging the reaction time could lead to its complete conversion to the

Table 5. Catalytic Performance of CP-900-1 in the Hydrogenation of Nitroarenes[a]

Entry	Substrate	Time (h)	Conversion (%)	Selectivity (%)
1		10	82.97	>99
2		10	92.47	>99
3		6	91.71	>99
4		6	>99	>99
5		3	>99	>99
6		3	92.00	>99
7		3	>99	79
8		3	84.49	>99
9		3	72.35	94.47

[a]Conditions: 30 mg catalyst, 0.25 mmol substrate, 2.5 mL of mixed solvent (V_{EtOH}/V_{H_2O} = 3:2), 3 MPa H_2, 140 °C.

corresponding anilines (entry 1). Notably, nitroarenes with electron-donating substituents required a longer reaction time to achieve higher yields (entry 2, entry 3) than nitroarenes with electron-withdrawing groups (entry 5). The selectivity of p-amino-styrene was only 79% when the nitroarene contained a double bond such as p-nitrostyrene, indicating that the CP-900−1 catalyst could catalyze the hydrogenation of carbon−carbon double bonds (entry 7).

For heterogeneous catalysis, the stability and recyclability of the catalyst are of great practical significance and are prerequisites for large-scale industrial applications. The CP-900−1 catalyst exhibited good retrievability and stability for the hydrogenation of nitrobenzene, with only a slight decrease in nitrobenzene conversion after 5 cycles (Figure 5).

4. CONCLUSIONS

In conclusion, N and P dual-doped metal-free catalysts were prepared through a direct pyrolysis method by employing sustainable biomass chitosan as both the carbon and nitrogen sources and phytic acid as the phosphorus source. N, P dual-doping significantly enhanced the catalytic activity of carbon materials. CP-900−1 catalyst showed superior catalytic efficiency for the hydrogenation of nitrobenzene. By exploring the relationship between the structure and activity of catalysts, it was found that doped P played a crucial role in promoting and regulating N doping. On the one hand, the doped P increased the content of N in the carbon material and affected the nitrogen doping mode to increase the content of pyridinic N; On the other hand, doped P facilitated the formation of
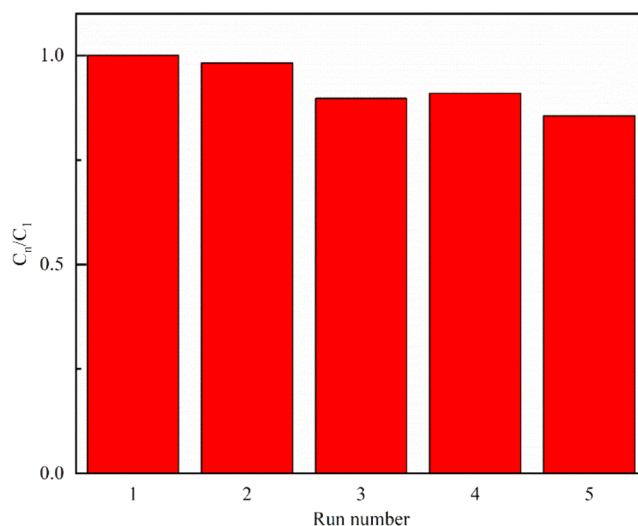

Figure 5. Cycle test of CP-900−1.

numerous P−C species and related active components. The excellent catalytic activity of the CP-900−1 catalyst should be attributed to the synergistic effects of pyridinic N, P−C species, and graphitic N. The doping of graphitic N facilitated the adsorption of nitrobenzene, while the presence of pyridinic N and P−C species was beneficial for the dissociation of H_2. Besides, the CP-900−1 catalyst exhibited good retrievability and cycling stability for the hydrogenation of nitrobenzene with little change in the conversion in 5 cycles.

■ ASSOCIATED CONTENT

ⓢ Supporting Information

The Supporting Information is available free of charge at https://pubs.acs.org/doi/10.1021/acsomega.4c02498.

> Calculations of nitrobenzene conversion and aniline selectivity; preparation details of the catalysts; solvent optimization; SEM and TEM images of the catalysts; high-resolution XPS spectra; and N_2 adsorption/ desorption isotherms and pore size distributions (PDF)

■ AUTHOR INFORMATION

Corresponding Author

Bowei Wang − *School of Chemical Engineering and Technology, Tianjin University, Tianjin 300350, P. R. China; Collaborative Innovation Center of Chemical Science and Engineering (Tianjin), Tianjin 300072, P. R. China; Tianjin Engineering Research Center of Functional Fine Chemicals, Tianjin 300350, P. R. China; Institute of Shaoxing, Tianjin University, Shaoxing, Zhejiang 312300, P. R. China;* ⓞ orcid.org/0000-0002-9400-0698; Email: bwwang@ tju.edu.cn

Authors

Zhaoshuo Jiang − *School of Chemical Engineering and Technology, Tianjin University, Tianjin 300350, P. R. China*

Yingchao Feng − *School of Chemical Engineering and Technology, Tianjin University, Tianjin 300350, P. R. China*

Yu Gou − *Department of Orthopaedic Surgery, Tianjin Hospital, Tianjin University, Tianjin 300211, P. R. China*

Ziyi Xia − *School of Chemical Engineering and Technology, Tianjin University, Tianjin 300350, P. R. China; Collaborative Innovation Center of Chemical Science and Engineering (Tianjin), Tianjin 300072, P. R. China; Tianjin Engineering Research Center of Functional Fine Chemicals, Tianjin 300350, P. R. China; Institute of Shaoxing, Tianjin University, Shaoxing, Zhejiang 312300, P. R. China*

Binwei Yuan − *Shaoxing Xingxin New Materials Co., Ltd, Shaoxing, Zhejiang 312300, P. R. China*

Syed Husnain Ali − *School of Chemical Engineering and Technology, Tianjin University, Tianjin 300350, P. R. China*

Xuejiao Rong − *School of Chemical Engineering and Technology, Tianjin University, Tianjin 300350, P. R. China*

Anni Guo − *School of Chemical Engineering and Technology, Tianjin University, Tianjin 300350, P. R. China*

Ligong Chen − *School of Chemical Engineering and Technology, Tianjin University, Tianjin 300350, P. R. China; Collaborative Innovation Center of Chemical Science and Engineering (Tianjin), Tianjin 300072, P. R. China; Tianjin Engineering Research Center of Functional Fine Chemicals, Tianjin 300350, P. R. China; Institute of Shaoxing, Tianjin University, Shaoxing, Zhejiang 312300, P. R. China;* ⓞ orcid.org/0000-0002-3442-5694

Complete contact information is available at:
https://pubs.acs.org/10.1021/acsomega.4c02498

Author Contributions

∇Z.J. and Y.F. contributed equally to this work.

Notes

The authors declare no competing financial interest.

■ ACKNOWLEDGMENTS

■ REFERENCES

(1) Aireddy, D. R.; Ding, K. Heterolytic Dissociation of H_2 in Heterogeneous Catalysis. *ACS Catal.* **2022**, *12* (8), 4707−4723.

(2) Liu, J.; Li, X.; Zhang, H.; Fu, H.; Zhao, N.; Chen, B. H.; Zhu, L. Synthesis of layered double hydroxide-supported platinum nanocatalyst for highly efficient and selective hydrogenation of nitroaromatics. *Mater. Chem. Phys.* **2022**, *287*, No. 126241.

(3) Saleh, T. A. Carbon nanotube-incorporated alumina as a support for MoNi catalysts for the efficient hydrodesulfurization of thiophenes. *Chem. Eng. J.* **2021**, *404*, No. 126987.

(4) Cui, X.; Surkus, A.-E.; Junge, K.; Topf, C.; Radnik, J.; Kreyenschulte, C.; Beller, M. Highly selective hydrogenation of arenes using nanostructured ruthenium catalysts modified with a carbon-nitrogen matrix. *Nat. Commun.* **2016**, *7*, No. 11326.

(5) Zhou, P.; Jiang, L.; Wang, F.; Deng, K.; Lv, K.; Zhang, Z. High performance of a cobalt-nitrogen complex for the reduction and reductive coupling of nitro compounds into amines and their derivatives. *Sci. Adv.* **2017**, *3* (2), No. e1601945.

(6) Kim, A. N.; Stoltz, B. M. Recent Advances in Homogeneous Catalysts for the Asymmetric Hydrogenation of Heteroarenes. *ACS Catal.* **2020**, *10* (23), 13834−13851.

(7) Jannsen, N.; Pribbenow, C.; Selle, C.; Drexler, H.-J.; Mueller, M.-A.; Medlock, J. A.; Bonrath, W.; Heller, D. Selective Catalysts for the Homogeneous Semi-Hydrogenation. *Adv. Synth. Catal.* **2023**, *365*, 4538−4543.

(8) Kratzer, E.; Schoetz, S.; Maisel, S.; Blaumeiser, D.; Antara, S. K.; Ewald, L.; Dotzel, D.; Haumann, M.; Goerling, A.; Korth, W.; Jess, A.; Retzer, T. Wilkinson-type catalysts in ionic liquids for hydrogenation of small alkenes: understanding and improving catalyst stability. *Catal. Sci. Technol.* **2023**, *13* (7), 2053−2069.

(9) Dang, S.; Yang, H.; Gao, P.; Wang, H.; Li, X.; Wei, W.; Sun, Y. A review of research progress on heterogeneous catalysts for methanol synthesis from carbon dioxide hydrogenation. *Catal. Today* **2019**, *330*, 61−75.

(10) Qu, R.; Junge, K.; Beller, M. Hydrogenation of Carboxylic Acids, Esters, and Related Compounds over Heterogeneous Catalysts: A Step toward Sustainable and Carbon-Neutral Processes. *Chem. Rev.* **2023**, *123* (3), 1103−1165.

(11) Li, M.; Li, W.; Yang, Y.; Yu, D.; Lin, J.; Wan, R.; Zhu, H. Remarkably efficient $Pt/CeO_2-Al_2O_3$ catalyst for catalytic hydrodeiodination of monoiodoacetic acid: Synergistic effect of Al2O3 and CeO_2. *Chemosphere* **2023**, *327*, No. 138515.

(12) Yu, J.; Muhetaer, A.; Gao, X.; Zhang, Z.; Yang, Y.; Li, Q.; Chen, L.; Liu, H.; Xu, D. Frontispiece: Highly Active Hydrogen-rich Photothermal Reverse Water Gas Shift Reaction on $Ni/LaInO_3$ Perovskite Catalysts with Near-unity Selectivity. *Angew. Chem., Int. Ed.* **2023**, *62* (28), No. e202382861.

(13) Shi, W.; Zhang, B.; Lin, Y.; Wang, Q.; Zhang, Q.; Su, D. S. Enhanced Chemoselective Hydrogenation through Tuning the Interaction between Pt Nanoparticles and Carbon Supports: Insights from Identical Location Transmission Electron Microscopy and X-ray Photoelectron Spectroscopy. *ACS Catal.* **2016**, *6* (11), 7844−7854.

(14) Pan, X.; Gao, X.; Chen, X.; Lee, H. N.; Liu, Y.; Withers, R. L.; Yi, Z. Design Synthesis of Nitrogen-Doped TiO_2@Carbon Nanosheets toward Selective Nitroaromatics Reduction under Mild Conditions. *ACS Catal.* **2017**, *7* (10), 6991−6998.

(15) Lu, X.; He, J.; Huang, L.; Qin, J.; Ma, Y.; Liu, X.; Zhao, W.; Liu, B.; Zhang, Z. Synergetic roles of pyridinic nitrogen and carbonyl sites in nitrogen-doped carbon for the metal-free transfer hydrogenation reactions. *Appl. Catal., B* **2023**, *324*, No. 122277.

(16) Rangraz, Y.; Heravi, M. M. Recent advances in metal-free heteroatom-doped carbon heterogonous catalysts. *RSC Adv.* 2021, *11* (38), 23725−23778.

(17) Jupp, A. R.; Stephan, D. W. New Directions for Frustrated Lewis Pair Chemistry. *Trends Chem.* 2019, *1* (1), 35−48.

(18) Gong, Y.; Li, M.; Li, H.; Wang, Y. Graphitic carbon nitride polymers: promising catalysts or catalyst supports for heterogeneous oxidation and hydrogenation. *Green Chem.* 2015, *17* (2), 715−736.

(19) Das, A.; Mondal, S.; Hansda, K. M.; Adak, M. K.; Dhak, D. A critical review on the role of carbon supports of metal catalysts for selective catalytic hydrogenation of chloronitrobenzenes. *Appl. Catal., A* 2023, *649*, No. 118955.

(20) Pei, X.; Jiao, H.; Fu, H.; Yin, X.; Luo, D.; Long, S.; Gong, W.; Zhang, L. Facile Construction of a Highly Dispersed Pt Nanocatalyst Anchored on Biomass-Derived N/O-Doped Carbon Nanofibrous Microspheres and Its Catalytic Hydrogenation. *ACS Appl. Mater. Interfaces* 2020, *12* (46), 51459−51467.

(21) Hu, X.; Long, Y.; Fan, M.; Yuan, M.; Zhao, H.; Ma, J.; Dong, Z. Two-dimensional covalent organic frameworks as self-template derived nitrogen-doped carbon nanosheets for eco-friendly metal-free catalysis. *Appl. Catal., B* 2019, *244*, 25−35.

(22) Liu, L.; Qiu, M.; Liu, S.; Ma, H.; Huang, Z.-Q.; Chang, C.-R. Design of Frustrated Lewis Pairs by Functionalizing N-Doped Graphene Edge with Tunable Activity for H_2 Dissociation. *J. Phys. Chem. C* 2023, *127* (14), 6714−6722.

(23) Chen, D.; Wu, L.; Nie, S.; Zhang, P. Solvent-free synthesis of N-doped carbon-based catalyst for high-efficient reduction of 4-nitrophenol. *J. Environ. Chem. Eng.* 2021, *9* (4), No. 105649.

(24) Fakir, A. A. E.; Anfar, Z.; Enneiymy, M.; Jada, A.; El Alem, N. Conjugated polymers templated carbonization to design N, S co-doped finely tunable carbon for enhanced synergistic catalysis. *Appl. Catal., B* 2022, *300*, No. 120732.

(25) Miao, L.; Duan, H.; Zhu, D.; Lv, Y.; Gan, L.; Li, L.; Liu, M. Boron ″gluing″ nitrogen heteroatoms in a prepolymerized ionic liquid-based carbon scaffold for durable supercapacitive activity. *J. Mater. Chem. A* 2021, *9* (5), 2714−2724.

(26) Gao, R.; Pan, L.; Lu, J.; Xu, J.; Zhang, X.; Wang, L.; Zou, J.-J. Phosphorus-Doped and Lattice-Defective Carbon as Metal-like Catalyst for the Selective Hydrogenation of Nitroarenes. *ChemCatChem* 2017, *9* (22), 4287−4294.

(27) Shang, S. S.; Gao, S. Heteroatom-Enhanced Metal-Free Catalytic Performance of Carbocatalysts for Organic Transformations. *ChemCatChem* 2019, *11* (16), 3728−3742.

(28) Xiong, W.; Wang, Z.; He, S.; Hao, F.; Yang, Y.; Lv, Y.; Zhang, W.; Liu, P.; Luo, H. Nitrogen-doped carbon nanotubes as a highly active metal-free catalyst for nitrobenzene hydrogenation. *Appl. Catal., B* 2020, *260*, No. 118105.

(29) Shan, J.; Sun, X.; Zheng, S.; Wang, T.; Zhang, X.; Li, G. Graphitic N-dominated nitrogen-doped carbon nanotubes as efficient metal-free catalysts for hydrogenation of nitroarenes. *Carbon* 2019, *146*, 60−69.

(30) Han, D.; Liu, Y.; Lv, Y.; Xiong, W.; Hao, F.; Luo, H.; Liu, P. In situ oxygen-induced zigzag graphene as metal-free catalyst for hydrogen activation in nitroarenes hydrogenation. *Carbon* 2023, *203*, 347−356.

(31) Li, J.; Wang, B.; Fang, W.; Li, Y.; Yan, X.; Xia, Z.; Chen, L. N, B dual-doped carbons as metal-free catalysts for hydrogenation of quinoline with formic acid. *Mol. Catal.* 2023, *540*, No. 113040.

(32) Zhang, H.; Zhang, C.; Zhang, Y.; Cul, P.; Zhang, Y.; Wang, L.; Wang, H.; Gao, Y. P/N co-doped carbon derived from cellulose: A metal-free photothermal catalyst for transfer hydrogenation of nitroarenes. *Appl. Surf. Sci.* 2019, *487*, 616−624.

(33) Hu, X.; Sun, X.; Song, Q.; Zhu, Y.; Long, Y.; Dong, Z. N,S co-doped hierarchically porous carbon materials for efficient metal-free catalysis. *Green Chem.* 2020, *22* (3), 742−752.

(34) Zhang, J.; Geng, W.; Shi, L.; Yang, C.; Zhang, X.; Geng, Y.; Hirani, R. A. K.; Xu, X.; Wei, J.; Jing, Y.; Zhang, S.; Zhang, H.; Wang, S.; Sun, H. One-pot synthesis of boron and nitrogen co-doped nanocarbons for efficient catalytic reduction of nitrophenols. *Chem. Eng. J.* 2022, *439*, No. 135733.

(35) Wen, G.; Diao, J.; Wu, S.; Yang, W.; Schoegl, R.; Su, D. S. Acid Properties of Nanocarbons and Their Application in Oxidative Dehydrogenation. *ACS Catal.* 2015, *5* (6), 3600−3608.

(36) Shang, S.; Chen, P.-P.; Wang, L.; Lv, Y.; Li, W.-X.; Gao, S. Metal-Free Nitrogen- and Boron-Codoped Mesoporous Carbons for Primary Amides Synthesis from Primary Alcohols via Direct Oxidative Dehydrogenation. *ACS Catal.* 2018, *8* (11), 9936−9944.

(37) Mu, Y.; Han, M.; Wu, B.; Wang, Y.; Li, Z.; Li, J.; Li, Z.; Wang, S.; Wan, J.; Zeng, L. Nitrogen, Oxygen-Codoped Vertical Graphene Arrays Coated 3D Flexible Carbon Nanofibers with High Silicon Content as an Ultrastable Anode for Superior Lithium Storage. *Adv. Sci.* 2022, *9* (6), No. 2104685.

(38) Guo, D.; Shibuya, R.; Akiba, C.; Saji, S.; Kondo, T.; Nakamura, J. Active sites of nitrogen-doped carbon materials for oxygen reduction reaction clarified using model catalysts. *Science* 2016, *351* (6271), 361−365.

(39) Chen, W.; Xu, L.; Tian, Y.; Li, H.; Wang, K. Boron and nitrogen co-doped graphene aerogels: Facile preparation, tunable doping contents and bifunctional oxygen electrocatalysis. *Carbon* 2018, *137*, 458−466.

(40) Yu, W.; Liu, L.; Gao, B.; Wang, L.; Yue, S. Pore structure of coal gasification fine slag based on nitrogen adsorption and nuclear magnetic resonance analysis. *J. Fuel Chem. Technol.* 2022, *50* (8), 966−973.

(41) Liu, R.; Li, F.; Chen, C.; Song, Q.; Zhao, N.; Xiao, F. Nitrogen-functionalized reduced graphene oxide as carbocatalysts with enhanced activity for polyaromatic hydrocarbon hydrogenation. *Catal. Sci. Technol.* 2017, *7* (5), 1217−1226.

(42) Yang, F.; Chi, C.; Wang, C.; Wang, Y.; Li, Y. High graphite N content in nitrogen-doped graphene as an efficient metal-free catalyst for reduction of nitroarenes in water. *Green Chem.* 2016, *18* (15), 4254−4262.

(43) Qu, Y.; Chen, T. Fullerene derivative supported Ni for hydrogenation of nitrobenzene: Effect of functional group of fullerene derivative. *Chem. Eng. J.* 2020, *382*, No. 122911.

(44) Zhang, G.; Tang, F.; Wang, X.; Wang, L.; Liu, Y.-N. Atomically Dispersed Co-S-N Active Sites Anchored on Hierarchically Porous Carbon for Efficient Catalytic Hydrogenation of Nitro Compounds. *ACS Catal.* 2022, *12* (10), 5786−5794.